AIAA JOURNAL
Vol. 32, No. 6, June 1994

Laser Interferometer Skin-Friction Measurements of Crossing-Shock-Wave/Turbulent-Boundary-Layer Interactions

T. J. Garrison* and G. S. Settles†
Pennsylvania State University, University Park, Pennsylvania 16802
and
N. Narayanswami‡ and D. D. Knight§
Rutgers University, Piscataway, New Jersey 08903

Wall shear stress measurements beneath crossing-shock-wave/turbulent boundary-layer interactions have been made for three interactions of different strengths. The interactions are generated by two sharp fins at symmetric angles of attack mounted on a flat plate. The shear stress measurements were made for fin angles of 7 and 11 deg at Mach 3 and 15 deg at Mach 3.85. The measurements were made using a laser interferometer skin-friction meter, a device that determines the wall shear by optically measuring the time rate of thinning of an oil film placed on the test model surface. Results of the measurements reveal high skin-friction coefficients in the vicinity of the fin/plate junction and the presence of quasi-two-dimensional flow separation on the interaction centerline. Additionally, two Navier-Stokes computations, one using a Baldwin-Lomax turbulence model and one using a k-ε model, are compared with the experimental results for the Mach 3.85, 15-deg interaction case. Although the k-ε model did a reasonable job of predicting the overall trend in portions of the skin-friction distribution, neither computation fully captured the physics of the near-surface flow in this complex interaction.

Nomenclature

C_f	= skin-friction coefficient based on incoming freestream conditions, τ_w/q_∞
$C_{f\infty}$	= flat plate skin-friction coefficient at $Z = 0$
M_∞	= incoming freestream Mach number
q_∞	= incoming freestream dynamic pressure, $(1/2)\rho_\infty U_\infty^2$
T_{aw}	= adiabatic wall temperature
X, Y, Z	= Cartesian coordinate directions
α	= fin angle of attack relative to freestream flow direction, deg
δ	= boundary-layer thickness
δ^*	= displacement thickness
θ	= momentum thickness
τ_w	= wall shear stress

Introduction

ALTHOUGH a knowledge of the surface shear stress distribution is quite important for understanding many types of flowfields, accurately obtaining such data, either experimentally or computationally, can be quite difficult. The level of difficulty increases considerably for high-speed, three-dimensional flows in which flow separation is present. This paper addresses the measurement of C_f, the skin-friction coefficient, in such a flowfield. The flowfield is that created by the confluence of two crossing oblique shock waves with a turbulent boundary layer. This type of interaction is a fundamental fluid dynamics problem that also has practical applications, most notably in the design of high-speed sidewall-compression inlets for airbreathing propulsion and missile fin configurations.

To date, the crossing-shock problem has undergone a limited amount of experimental and computational study. Early on, the available experimental data were quite limited, consisting mainly of surface pressures and limiting surface streamline patterns.[1–5] This limitation in data made it difficult to understand the physics of these interactions and also limited the computational fluid dynamics (CFD) code validation efforts. Recently, a semiquantitative flowfield model based on flow visualization of a strong crossing-shock interaction has been presented[6] and later revised and compared with computational results.[7] The comparison of the experimentally observed flowfield with the computational results showed reasonable agreement away from the surface, but significant differences were found near the model surface. These near-wall differences were attributed to inadequacies of the turbulence models used. The experimental flowfield model was then further revised and extended to cover a range of interaction strengths.[8] This flowfield model provided fundamental insight into the structure of the crossing-shock interaction, revealing that it is dominated by a large, viscous, separated-flow region. However, because the flowfield model is semiquantitative, it conveys only partial information on the crossing-shock interaction.

Thus, there is a need to obtain quantitative experimental data for the augmentation of the flowfield model and to strengthen the experimental basis against which CFD turbulence models are evaluated. To address this need, skin-friction measurements were recently made for three crossing-shock interactions of differing strengths. Because the accurate measurement of C_f in complex flows is quite difficult, no such data currently exist for the crossing-shock interaction.

The C_f data presented in this paper were obtained using a laser interferometer skin friction (LISF) meter. The LISF meter's ability to successfully measure skin friction in complex, high-speed flows has been previously demonstrated by Kim,[9] Kim and Settles,[10,11] and Kim et al.[12] As part of the present study, both the LISF instrument and the data-reduction procedure originally used by Kim have been revised to enhance their performance in high-shear flows.

The goal of this study is to use the enhanced LISF meter to obtain reliable skin-friction data within the crossing-shock interac-

Received June 24, 1993; presented as Paper 93-3072 at the AIAA 24th Fluid Dynamics Conference, Orlando, FL, July 6–9, 1993; revision received Nov. 22, 1993; accepted for publication Nov. 29, 1993.

*Graduate Research Assistant; currently Assistant Professor, Department of Mechanical Engineering, Louisiana State University. Student Member AIAA.

†Professor, Department of Mechanical Engineering, and Director, Gas Dynamics Laboratory. Associate Fellow AIAA.

‡Research Staff Member; currently Research Staff, Shock Wave Research Center, Tohoku University, Sendai, Japan. Member AIAA.

§Professor, Department of Mechanical and Aerospace Engineering. Associate Fellow AIAA.

tion. Such data will serve two major purposes. The first is to help better understand the physics of the crossing-shock interaction. The second is to provide data that will serve as a benchmark for turbulence modeling and CFD code validation.

Experimental Techniques

Wind-Tunnel Facility and Test Conditions

The experiments were performed in the Pennsylvania State University Gas Dynamics Laboratory's Supersonic Wind Tunnel Facility, which is an intermittent blowdown tunnel with a test section size of $15 \times 17 \times 61$ cm. This facility has a unique variable Mach number capability over the range of Mach 1.5–4.0 by way of an asymmetric sliding-block nozzle. The experiments described in this paper were carried out at Mach numbers of 3 and 3.85, with typical tunnel operating conditions consisting of a stagnation pressure of 750 kPa at Mach 3 and 1500 kPa at Mach 3.85, a stagnation temperature of 295 K, and a unit Reynolds number of approximately 80×10^6/m at both Mach numbers.

Test Model

Figure 1 shows the model geometry used for the crossing-shock experiments, consisting of two vertical fins, each at angle of attack α, mounted on a horizontal flat plate. The flat plate generates an equilibrium, nearly adiabatic, zero-pressure-gradient turbulent boundary layer that interacts with the two crossing oblique shock waves generated by the fins. The incoming properties of the boundary layer are $\delta \approx 3.5$ mm, $\delta^* \approx 1.12$ mm, and $\theta \approx 0.13$ mm at both test Mach numbers. The fin leading edges are located 21.3 cm downstream of the plate leading edge, with a transverse distance between them of 9.4 cm for the Mach 3 tests and 10.6 cm at Mach 3.85. The height of the fins is 8.25 cm, a value large enough to be effectively "semi-infinite." Both fins can be positioned at angles of attack up to 15 deg. The fin angles were carefully set using a protractor with an accuracy of $\pm$ 0.1 deg. For the experiments described in this paper, three distinct combinations of Mach number and fin angles were examined. Symmetric fin angles of 7 and 11 deg were tested at Mach 3, and fin angles of 15 deg were tested at Mach 3.85.

As part of the LISF analysis one must accurately know the viscosity of the oil film at all times. Because the test model temperature changes during the course of a wind-tunnel run, the oil viscosity also changes with run time. To account for this variation, an array of embedded thermocouples is installed in the flat plate. The locations of the thermocouples are determined based on the desired LISF measurement locations. The output of these thermocouples, along with the known temperature-viscosity calibration for the silicone oil, are then used to determine the oil viscosity at any instant in time.

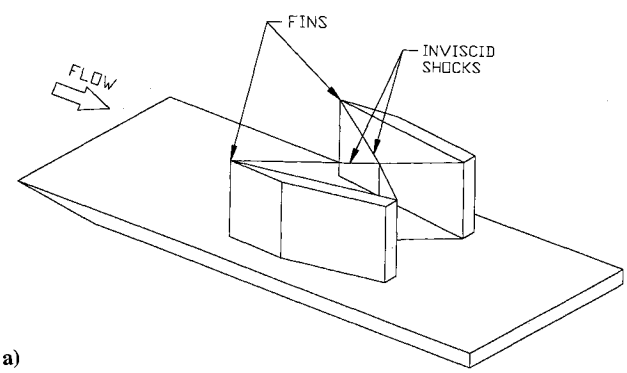

Fig. 1 Model geometry: a) perspective view and b) top view.

Kerosene Lampblack Surface Traces

To perform LISF skin-friction measurements within a three-dimensional flowfield, one must know a priori the direction of the shear stress vector τ_w. The direction of this vector can easily be determined through the use of surface flow visualization. For the crossing-shock experiments, the surface flow visualization patterns of the interaction "footprint" were recorded by applying a mixture of kerosene and lampblack to the surface of the flat plate. Because of its volatility, the kerosene evaporates shortly after the pattern has formed, leaving the dry lampblack pigment on the surface. This lampblack pattern is then removed from the model surface using large squares of matte adhesive tape. A more detailed description of this method can be found in Ref. 13.

LISF Technique

The LISF meter was originally invented by Tanner and Blows[14] for use in low-speed flows. The technique was further enhanced by Tanner,[15,16] Tanner and Kulkarni,[17] Monson and Higuchi,[18] Monson et al.,[19] Monson,[20] Westphal et al.,[21] and most recently by Kim,[9] Kim and Settles,[10,11] and Kim et al.[12] The basic principle of operation of the LISF meter is to optically measure the time rate of thinning of an oil film placed on a test surface subject to aerodynamic shear. The rate of thinning of the oil film is determined using optical interference and can be related to the applied shear stress through lubrication theory. In this way, the shear stress can be determined without any knowledge of the overlying flow properties (i.e., only properties of the oil and not properties of the outer flow are required to determine the shear).

Although the LISF meter was originally used for low-speed flows, Monson et al.[19] were the first to attempt LISF measurements in supersonic flows. In general, the principle of operation of the instrument itself is not limited by the speed of the outer flow. Nonetheless, practical difficulties do arise as the magnitude of the shear stress grows. The most challenging difficulty is the generation of waves that form on the oil surface. These surface waves persist in high-shear environments until the oil film becomes quite thin, thus limiting the useful output signal of the LISF meter. Continued improvements in the optics and data reduction technique, along with studies of the surface wave phenomena by Murphy and Westphal,[22] have extended the practical working range of the instrument significantly. Kim,[9] Kim and Settles,[10,11] and Kim et al.[12] used the instrument extensively in high-speed flows, successfully measuring the skin-friction distributions beneath swept shock/boundary-layer interactions. The instrument and data-reduction algorithm used by Kim have subsequently been revised and enhanced during this study, as part of an ongoing effort to improve the LISF meter for complex, high-speed flows. Although the maximum shear stress that the current LISF instrument can measure depends on both the oil viscosity used and the flow conditions at the measurement location, it was found that shear stresses up to approximately 700 N/m^2 could be successfully measured.

Figure 2 shows a schematic of the LISF instrument used in this study. In this arrangement, the beam from a 5-mW helium-neon laser first passes through an iris diaphragm followed by a 10X microscope objective and a focusing lens. The beam is then turned downward by an optical flat, passing through a second focusing lens and finally through a clear acrylic window in the wind-tunnel ceiling. The microscope objective, in combination with the two focusing lenses that follow, is used to produce a precisely focused beam on the oil film surface. By adjusting the separation between the microscope objective and the first focusing lens, a sharply focused laser spot less than 0.25 mm in diameter can be generated on the oil film. The optical flat is adjusted to direct the beam nearly normal to the plate surface, resulting in an incidence angle of 1–2 deg. The optical flat also serves to significantly reduce the power of the laser beam, since most of the incident beam passes through the flat and strikes a beam stop.

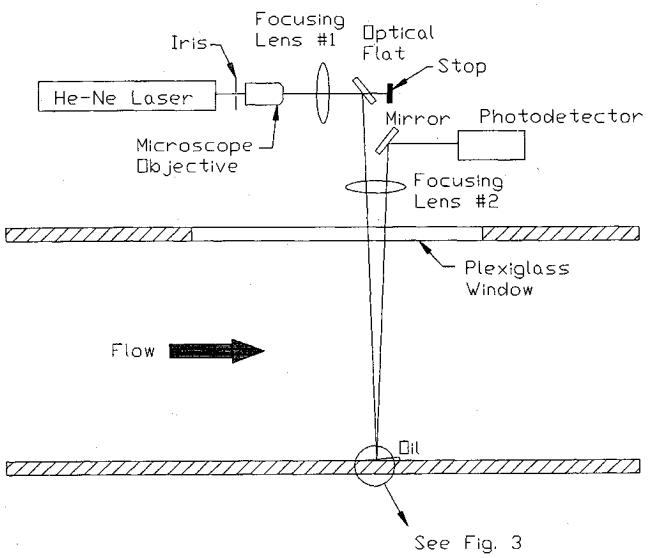

Fig. 2 Schematic of LISF instrument setup.

Referring to Fig. 3, which is an enlargement of the oil film in Fig. 2, a portion of the incident laser beam is reflected from the top surface of the oil whereas the remainder of the beam passes through the oil and reflects from the polished model surface. The two reflected beams then pass out through the acrylic window and back through focusing lens no. 2. This lens collects the two reflected beams (which are slightly diffused by the oil and plate surfaces) and refocuses them on a photodetector. Because these two beams have traveled different optical path lengths, they generate an interference pattern that is recorded by the photodetector. During the course of a wind-tunnel run, the applied aerodynamic shear thins the oil and generates a corresponding time-variant interference pattern. This pattern is sensed by the photodetector and digitally recorded using a data acquisition system. Figure 4 shows a sample of such an interference pattern generated during the present crossing-shock skin-friction measurements.

Data Reduction Method

As mentioned, the LISF data-reduction method has currently been revised and enhanced for better results in high-shear flows. In low-speed flows, many interference fringes can be obtained, allowing a simple data-reduction approach. Detailed discussions of the data reduction process in such cases can be found in Refs. 14, 15, and 18. For high-speed flows, however, the surface waves significantly reduce the portion of the interference signal that is usable. Furthermore, time-variant model temperatures result in oil viscosity variations that must be accounted for in the data-reduction method. Past data reduction algorithms for high-shear flows[10,12,19,20] were based on modifications to the established low-speed algorithms to account for this variable oil viscosity. In these methods, only the peaks of the experimentally recorded interference fringes were used to determine the shear stress. However, as the shear stress increases, the number of available peaks in the LISF signal decreases. This results in a shear stress determination based on a limited amount of data.

To enhance the method for use in high-speed flows, a new data-reduction technique was developed that uses the entire LISF signal to determine the shear stress. In this method, an analytical expression for the time-variant phase difference between the two beams was derived. This equation for the phase difference contains a single unknown constant τ_w. The value of τ_w is determined by taking the cross-correlation between the actual LISF signal and the analytical phase equation, with the actual value of the shear stress being the value that yields the maximum correlation.

Because a detailed description of the revised data-reduction process is quite lengthy, it cannot be included as part of this paper. The main purpose of this paper is to present the results of the method as applied to the study of crossing-shock/boundary-layer interactions. A paper describing the enhancements to the instrument and data reduction is planned in the near future.[23]

Calibration and Error Analysis

A detailed calibration of the LISF instrument was performed for a flat plate compressible turbulent boundary layer. The results were then compared with several methods commonly used to estimate flat plate C_f (i.e., the Van Driest II skin-friction theory,[24] an eddy-viscosity boundary-layer code,[25] and the extraction of C_f from measured velocity profiles using the Van Driest transformation coupled with the wall-wake similarity law[26]). These comparisons were made over a Mach number range from 2.4 to 4.0. Referring to Fig. 5, over this Mach number range, the maximum deviation between the LISF results and the "standard" calibration values was less than 10%, demonstrating that the LISF instrument can accurately predict the C_f distribution for a flat plate boundary

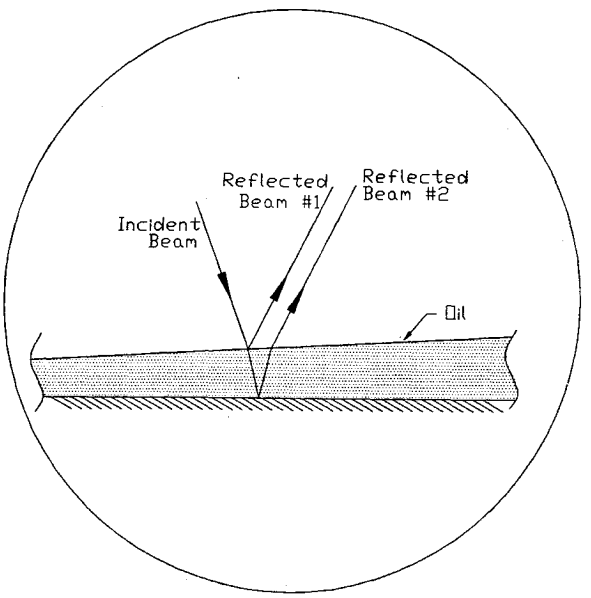

Fig. 3 Magnified view of oil film shown in Fig. 2.

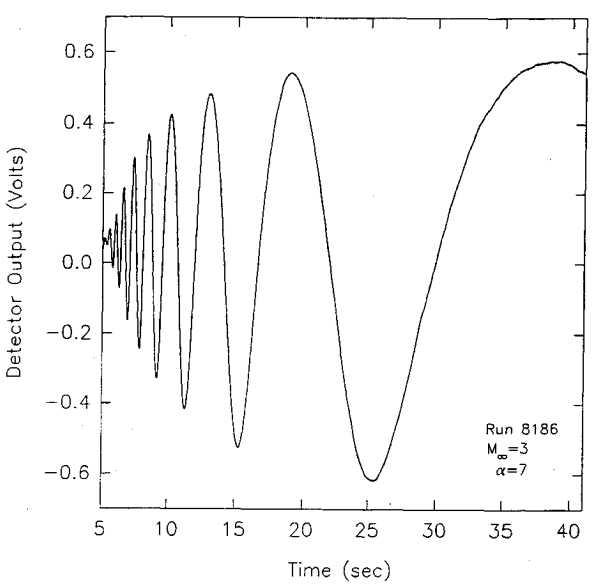

Fig. 4 Sample LISF interference signal.

layer. Although the data point at Mach 4 appears to be somewhat low, if error bars are included on the "standards" (which themselves are only accurate to the order of ±10% at best), then the LISF result falls within this error band. In fact, as discussed in a following section, the Mach 4 flat plate C_f values predicted by the two computations described in this paper bracket the LISF value.

Based on improvements to both the LISF meter and the data-reduction process, the difference between the LISF results and the "standard" values has been reduced below that of previous applications of the instrument in high-speed flows.[9–11] Within the complex crossing-shock flowfield, however, no calibration standard exists with which to judge the absolute accuracy of the LISF skin-friction measurements. Thus, the error bars for the data presented in the following sections are actually repeatability bars given as 95% confidence intervals based on repeated measurements for a given location on the model surface. In general, for each measurement position, multiple wind-tunnel runs were performed until the 95% confidence band was within ±10% of the mean shear value. This typically required between 4 to 8 test runs per measurement location.

Results and Discussion

Mach 3, 7-Degree Interaction

Figure 6 shows the measured C_f distribution for the Mach 3, α = 7-deg interaction, along with the corresponding kerosene-lampblack surface flow pattern. The C_f measurements were taken along the centerline of the interaction and along a spanwise cut from the centerline out to the fin location. The location of this spanwise cut is indicated by "SC" in the surface flow pattern, as is the streamwise location of the inviscid shock-crossing point, "IC." As shown in Fig. 1b, the origin of the coordinate system is located on the centerline of the interaction at the fin leading edges.

Along the centerline of the Mach 3, α = 7-deg interaction, the skin-friction coefficient begins at the flat plate level and then decreases steadily through the interaction, finally leveling off at the exit of the interaction at a value of approximately half the incoming level. It is interesting to compare the measured centerline C_f distribution to the surface flow pattern. Upstream, in the freestream flow, the surface flow streamlines are parallel and the corresponding C_f distribution is flat and equal to the flat plate value $C_{f\infty}$. Inside the interaction, the surface flow streamlines converge toward the centerline and the C_f correspondingly decreases steadily. In this portion of the interaction, the incoming boundary layer undergoes an adverse pressure gradient due to the compression caused by the crossing shocks. This pressure gradient retards the flow and thus lowers the wall shear.

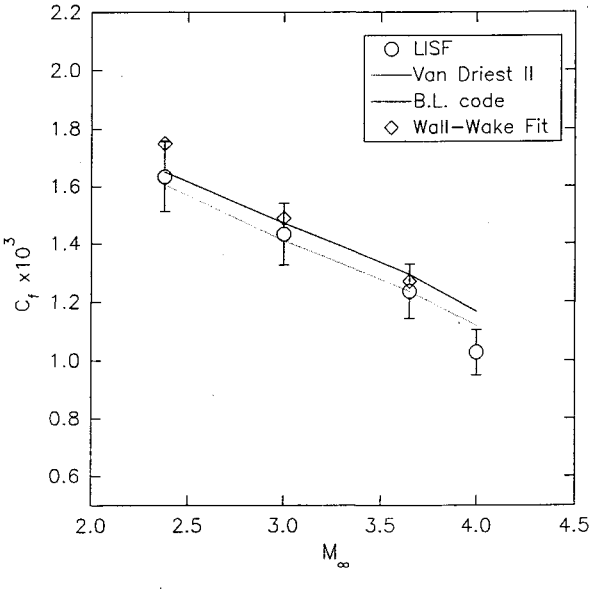

Fig. 5 Comparison of LISF flat plate C_f results.

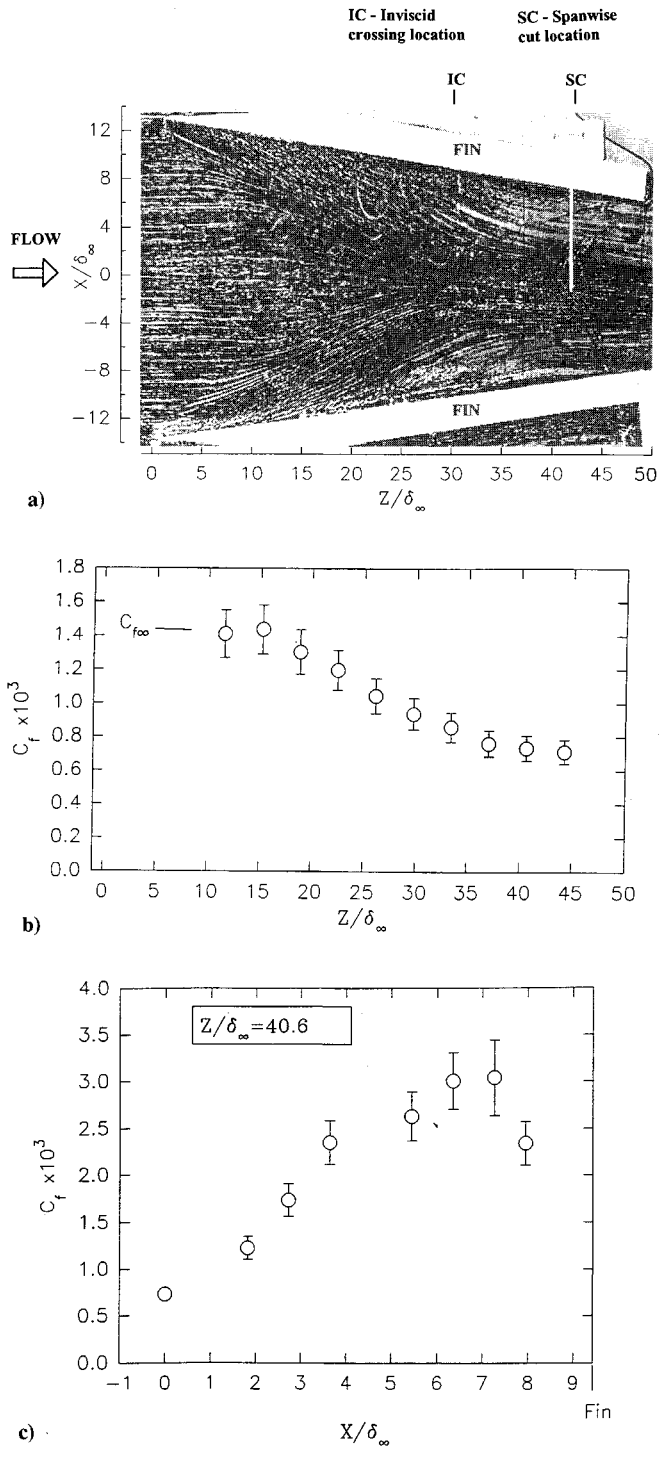

Fig. 6 Skin-friction coefficients for the Mach 3, 7-deg interaction: a) surface flow pattern, b) skin-friction distribution along the interaction centerline, and c) skin-friction distribution along a spanwise cut at Z/δ_∞ = 40.6.

Further downstream, beyond the inviscid shock crossing location, the surface flow streamlines turn once again parallel to the interaction centerline and remain so throughout the balance of the interaction. Over this region the C_f distribution also becomes flat once again. Thus, the measured C_f distribution corresponds quite well with the apparent physics of the surface flow pattern. As will be seen in the other two interaction cases as well, such surface flow patterns can be used to provide considerable physical insight into the behavior of the skin-friction distribution. This is not surprising, since the limiting surface streamlines are, in fact, a direct result of the wall shear stress vector field.

In the spanwise cut, Fig. 6c, C_f begins at the centerline value and increases significantly as the fin is approached. The peak C_f occurs very near the fin/plate junction and is associatedwith a line of flow attachment in the surface flow pattern. (Reference 8 gives a thorough discussion of the various topological features present within the crossing-shock surface flow pattern.) The peak C_f value in this spanwise cut is more than double the incoming flat plate value.

Mach 3, 11-Degree Interaction

Figure 7 shows results of the C_f measurements for the Mach 3, α = 11 deg interaction. Data are presented along the interaction centerline and along two spanwise cuts whose locations are marked in the corresponding surface flow pattern. The centerline C_f distribution begins at the flat plate value and drops off rapidly in the initial portion of the interaction, tending toward zero near $Z/\delta_\infty = 27.5$. At this location a two-dimensional-type centerline separation appears to occur in which the wall shear goes to zero. Because the centerplane of the symmetric crossing-shock interaction is a plane of symmetry, the flow in this plane behaves in a quasi-two-dimensional manner. Examination of the surface flow pattern clearly shows the presence of a separation bubble centered on the plane of symmetry at the location where the measured C_f is near zero. Notice that this pattern differs distinctly from the pattern of the weaker interaction shown earlier in Fig. 6 for which no flow separation occurs on the interaction centerline.

Downstream of the separation bubble, the wall shear stress rises rapidly from near zero at the separated region to some 25% greater than the incoming flat plate value and then levels off near the rear of the interaction. The rapid rise in C_f downstream of the separation bubble is analogous to the reacceleration of a two-dimensional flow that occurs beyond the attachment point downstream of a two-dimensional separation bubble. It should be pointed out that, along the centerline of the crossing-shock interaction, especially in the vicinity of the separation bubble, the flow pattern has been observed to exhibit unsteadiness.[5] Thus, one may question how this flowfield unsteadiness impacts the LISF measurements. Murphy and Westphal[22] have addressed this issue in detail and have shown that the LISF technique can accurately measure C_f under such circumstances.

In the spanwise direction, Fig. 7c, the shear stress distributions are very similar to those of the α = 7-deg interaction. The C_f measurements start at the centerline value and then reach a peak near the fin, with the peak value being significantly higher than the incoming flat plate value. By comparing the two spanwise cuts, it is observed that the peak value increases as one moves further downstream. For the spanwise cut at $Z/\delta_\infty = 30.0$, the peak C_f is 2.6 times the incoming value, whereas for the cut at $Z/\delta_\infty = 37.5$, the peak is 3.1 times the incoming value.

Mach 3.85, 15-Degree Interaction

The C_f distributions for the strongest interaction studied, the Mach 3.85, α = 15 deg case, are shown in Fig. 8. In addition to the experimentally recorded C_f values along the interaction centerline and a spanwise cut, two computational solutions are presented for comparison. These computations use two different turbulence models. One computation, carried out by Narayanswami and Knight, uses the Baldwin-Lomax algebraic eddy viscosity model. The other, using a k-ε two-equation model, was carried out by Horstman. Both computations solve the full three-dimensional mean compressible Reynolds-averaged Navier-Stokes equations. Because of the symmetry of the crossing-shock interaction, only half of the experimental domain was computed. The incoming boundary-layer profile for both computations was set to match the experimental profile. Also, the wall temperature was set to 1.06 T_{aw} to match the experimental value. For the Baldwin-Lomax computation, a grid size of $44 \times 66 \times 66$ was used in the X, Y, and Z directions, respectively, whereas for the k-ε computation a grid size of $40 \times 64 \times 79$ was used. The grid spacing of both computations varied spatially, with grid points being concentrated near the plate and fin surface. The grid spacings were determined based on a previous grid-refinement study for a Mach 8.3 crossing-shock interaction.[27] A detailed description of the computation using the Baldwin-Lomax model can be found in Ref. 7. Details of the k-ε computation for this interaction have yet to be published, but a description of the same model applied to a Mach 8.3, 15-deg crossing-shock interaction can be found in Ref. 28. The interested reader should consult these references if additional information on the computations is desired.

Consider first the experimental C_f distribution along the interaction centerline, shown in Fig. 8b. The C_f distribution again begins at the incoming flat plate value and drops sharply through the initial portion of the interaction. As in the Mach 3, 11-deg case, the

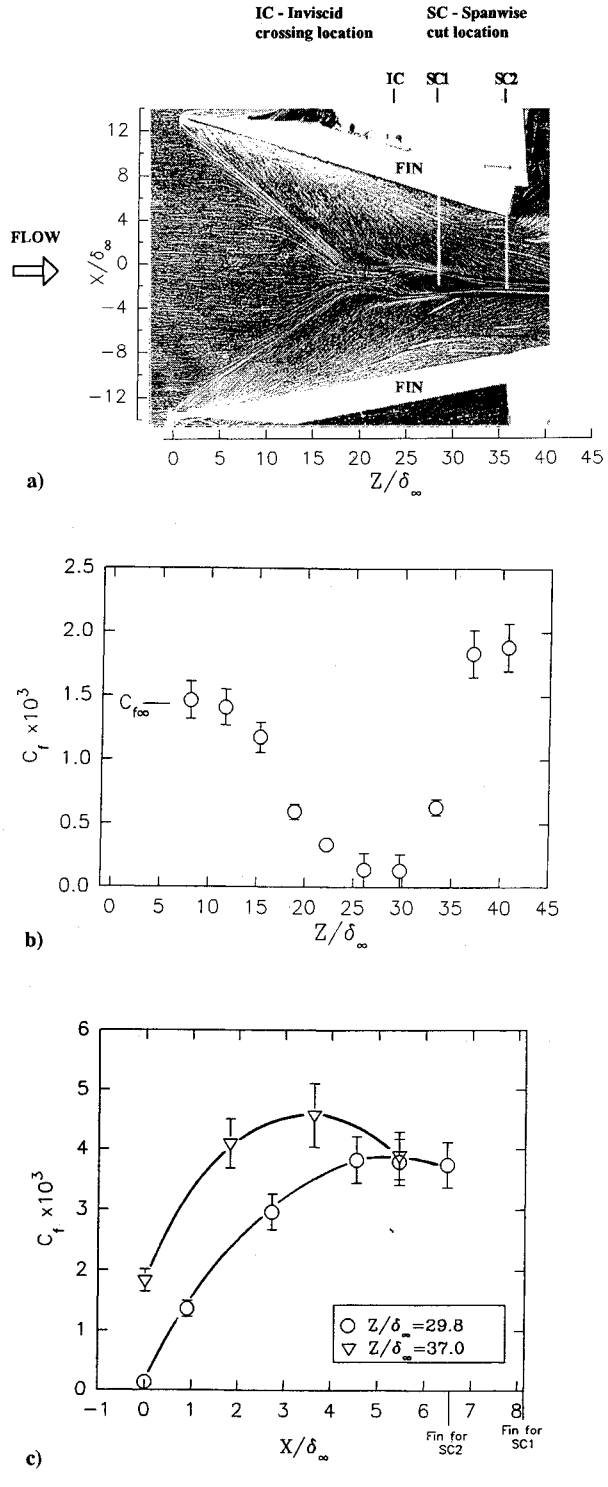

Fig. 7 Skin-friction coefficients for the Mach 3, 11-deg interaction: a) surface flow pattern, b) skin-friction distribution along the interaction centerline, and c) skin-friction distribution along spanwise cuts at Z/δ_∞ = 29.8 and 37.0.

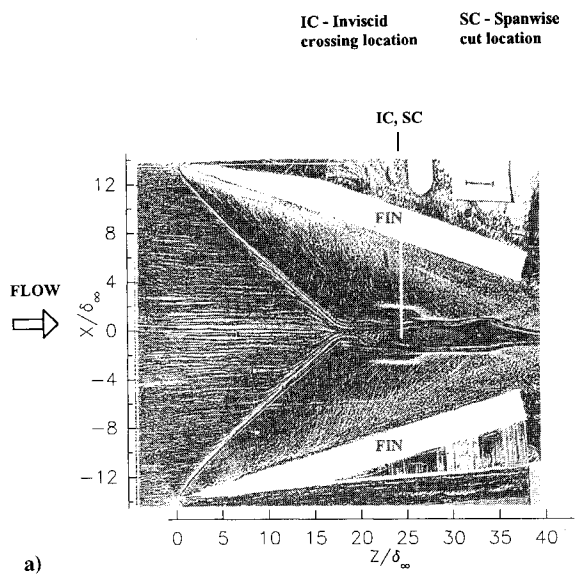

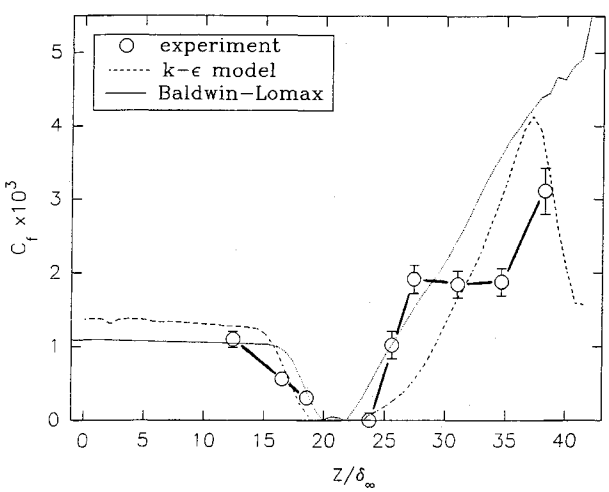

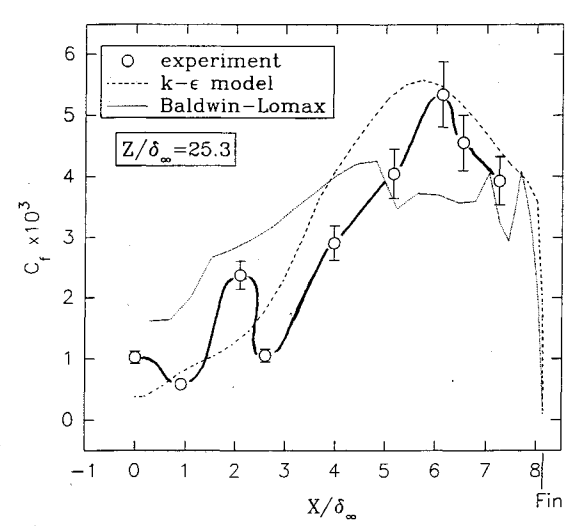

Fig. 8 Measured and computed skin-friction coefficients for the Mach 3.85, 15-deg interaction: a) surface flow pattern, b) skin-friction distribution along the interaction centerline, and c) skin-friction distribution along a spanwise cut at $Z/\delta_\infty = 25.3$.

shear stress goes to zero on the interaction centerline and the onset of a corresponding separation bubble is observed in the surface flow pattern. Downstream of the separation, the shear initially rises quite drastically, then levels off, forming a plateau, and then rises again further downstream. Note that the plateau in the C_f distribution directly corresponds to the region of the surface flow pattern where the streamlines near the centerline run nearly parallel to it. In this region there is little change in the surface pattern and thus little change in the C_f values. Once again this illustrates how the measured C_f distribution relates directly to the observed surface flow pattern. At the end of the interaction the centerline C_f has risen to nearly three times the incoming value.

The spanwise cut for this interaction, Fig. 8c, was selected at the inviscid crossing location, unlike the two preceding cases, to gain a better understanding of the effects in the vicinity of the crossing point. Beginning at the interaction centerline, the measured C_f first decreases, reaching a local minimum at the outside edge of the separation bubble ($X/\delta_\infty = 0.85$). The shear stress then increases to a local maximum just before the secondary separation line and then drops to another local minimum at the secondary separation line ($X/\delta_\infty = 2.6$). The shear then rises dramatically as the fin is approached, reaching a peak value 5.5 times $C_{f\infty}$ at the primary flow attachment line.

In this spanwise cut, in the region from $X/\delta_\infty = 0.0$ to 2.6 where the local minimum and maximum occur, one might question how the C_f distribution can be inferred from the limited number of data points taken. Indeed, an alternative interpretation might attribute this merely to data scatter. Thus it should be noted that, by examining the oil film fringe distribution at the end of a wind-tunnel run, one can determine the general nature of the C_f distribution. This is illustrated in Fig. 9, which shows an interference pattern obtained at the end of a run in a region for which the wall shear varied in the spanwise direction. Regions in which the fringes are widely spaced represent regions of high shear, whereas regions in which the fringes are closely spaced represent lower shear. By observing the oil fringe pattern, the qualitative shape of the C_f distribution can be obtained a priori. For the spanwise distribution just described, an initial run was performed to determine the shape of the C_f distribution. Then data points were purposely taken at the local minima and maxima to define the exact shape of the distribution. In this way, the distribution was quantified with the minimum number of measurements.

Next, examining the computational results for the centerline C_f, Fig. 8b, it can be seen that both solutions predict the general trend of the data in the upstream region of the interaction; namely, they show the C_f approaching zero in the same vicinity where the experimental data points do so. Further downstream, however, the computational comparison with the data deteriorates. Neither computation predicts the plateau observed experimentally, and toward the rear of the interaction, the computational results are drastically different from the experimental values and each other. Here, differences between the experiments and computations are as much as a factor of 2. Moreover, it is not surprising that the computations fail to accurately predict the centerline C_f distribution, since the com-

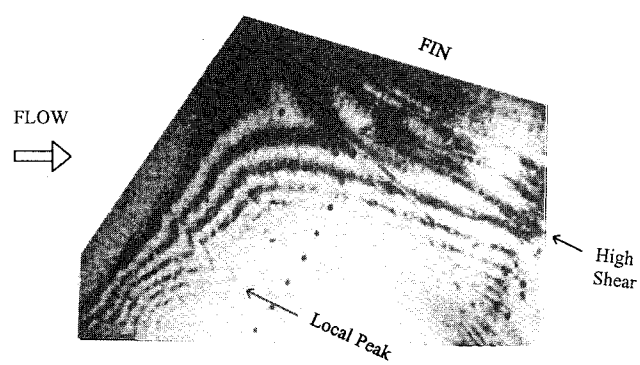

Fig. 9 Oil fringe pattern.

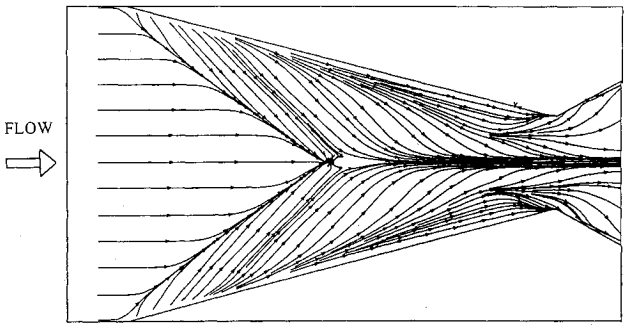

Fig. 10 Surface streamline pattern predicted for the Mach 3.85, 15-deg interaction by the computation employing the Baldwin-Lomax model.

puted surface flow pattern, shown in Fig. 10, has been shown to be significantly different than the experimental pattern in this region.[7] Since the experimental results have shown a direct correlation between the surface flow pattern and the quantitative shear stress distribution, failure of the computations to predict the surface pattern is a direct indication of inadequacies in the turbulence models used. In general, neither turbulence model is capable of describing the complex physics of the crossing-shock interaction along its centerline. It is useful to note that, even though both computations started with the same incoming experimental boundary-layer profile (measured 3.5 cm upstream of the fin leading edges), they predicted different flat plate C_f values just ahead of the interaction. The predicted flat plate C_f values bracket the LISF result. This suggests that the Mach 4 data point in Fig. 5 may appear to be low because of inaccuracies in the computed standard values.

Comparing the computed spanwise distributions with the experimental results, Fig. 8c, shows that the k-ε model predicts the gross behavior of the distribution but fails to resolve some of the key physics. Neither model is capable of predicting the complex measured variations in the shear stress close to the centerline. Further out toward the fin, the k-ε model predicts the peak value to within the experimental uncertainty, whereas the Baldwin-Lomax model suffers from spurious fluctuations. These fluctuations are most likely due to well-known problems that the Baldwin-Lomax model has in selecting the proper mixing length.

In general, the computations predict only portions of the overall behavior of the measured shear stress distributions. Even where the computations do predict the general trends, they tend to "wash out" the more intricate details of the flow physics. These results seem to indicate that the simplified turbulence models used in this study are of limited use in accurately predicting the surface transport properties of such a complex flow. Away from the surface, where the flowfield is mainly inviscid and rotational, the computations have previously shown reasonable success in matching the experimental results.[7,27]

Conclusions

An experimental study of the skin-friction distribution beneath crossing-shock/boundary-layer interactions of various strengths has been carried out. In addition, a comparison of the experimental results with two computational solutions has been made for the strongest interaction measured experimentally. Significant conclusions obtained during the course of this study are enumerated as follows:

1) A laser interferometer technique has been successfully used to measure the skin-friction distribution beneath complex crossing-shock/boundary-layer interactions.

2) For all but the weakest interaction, the flow in the vicinity of the interaction centerline undergoes a local quasi-two-dimensional separation.

3) A strong peak in the C_f distribution is observed near the fin/plate junction, coinciding with the primary flow attachment line.

4) The magnitude of this peak C_f increases in the streamwise direction.

5) The surface flow patterns were found to correlate directly with the measured C_f distributions, providing valuable insight into the behavior of the wall shear stress distribution.

6) Overall, the Navier-Stokes computation using a k-ε model did a better job of predicting the wall shear than the one using a Baldwin-Lomax model. However, both models failed to accurately predict important aspects of the measured C_f distributions.

7) For accurate prediction of surface transport properties in complex flows such as the crossing-shock/boundary-layer interaction, significant improvements in present-generation turbulence models appear to be needed.

Acknowledgments

This work was supported by the Air Force Office of Scientific Research through AFOSR Grant 89-0315, monitored by L. Sakell, and by NASA Ames Grant NGT-50952, monitored by C. C. Horstman. The authors would like to thank C. C. Horstman for providing the computational solution employing the k-ε turbulence model and for his extensive cooperation in this study.

References

[1]Mee, D. J., Stalker, R. J., and Stollery, J. L., "Glancing Interactions Between Single and Intersecting Oblique Shock Waves and a Turbulent Boundary Layer," *Journal of Fluid Mechanics*, Vol. 170, Sept. 1986, pp. 411–433.

[2]Batcho, P. F., Ketchum, A. C., Bogdonoff, S. M., and Fernando, E. M., "Preliminary Study of the Interactions Caused by Crossing Shock Waves and a Turbulent Boundary Layer," AIAA Paper 89-0359, Jan. 1989.

[3]Hingst, W. R., and Williams, K. E., "Interaction of Two Glancing, Crossing Shock Waves with Turbulent Boundary Layers at Various Mach Numbers," NASA TM 103740, 1991.

[4]Bogdonoff, S. M., and Stokes, W. L., "Crossing Shock Wave Turbulent Boundary Layer Interactions—Variable Angle and Shock Generator Length Geometry Effects at Mach 3," AIAA Paper 92-0636, Jan. 1992.

[5]Poddar, K., and Bogdonoff, S. M., "A Study of the Unsteadiness of Crossing Shock Wave Turbulent Boundary Layer Interactions," AIAA Paper 90-1456, June 1990.

[6]Garrison, T. J., and Settles, G. S., "Flowfield Visualization of Crossing Shock-Wave/Boundary Layer Interactions," AIAA Paper 92-0750, Jan. 1992.

[7]Garrison, T. J., Settles, G. S., Narayanswami, N., and Knight, D., "Structure of Crossing Shock-Wave/Turbulent Boundary Layer Interactions," *AIAA Journal*, Vol. 31, No. 12, 1993, pp. 2204–2211.

[8]Garrison, T. J., and Settles, G. S., "Interaction Strength and Model Geometry Effects on the Structure of Crossing-Shock Wave/Turbulent Boundary-Layer Interactions," AIAA Paper 93-0780, Jan. 1993.

[9]Kim, K.-S., "Skin Friction Measurements by Laser Interferometry in Supersonic Flows," Ph.D. Dissertation, Mechanical Engineering Dept., Pennsylvania State Univ., University Park, PA, 1988.

[10]Kim, K.-S., and Settles, G. S., "Skin-Friction Measurements by Laser Interferometry," *A Survey of Measurements and Measurement Techniques in Rapidly Distorted Compressible Boundary Layers*, edited by H. H. Fernholz, A. J. Smits, and J. P. Dussauge, AGARDograph 315, Nov. 1988, pp. 4.1–4.8.

[11]Kim, K.-S., and Settles, G. S., "Skin Friction Measurements by Laser Interferometry in Swept Shock/Boundary-Layer Interactions," *AIAA Journal*, Vol. 28, No. 1, 1990, pp. 133–139.

[12]Kim, K.-S., Lee, Y., Alvi, F. S., and Settles, G. S., "Skin-Friction Measurements and Computational Comparison of Swept Shock/Boundary Layer Interactions," *AIAA Journal*, Vol. 29, No. 10, 1991, pp. 1643–1650.

[13]Settles, G. S., and Teng, H. Y., "Flow Visualization Methods for Separated Three-Dimensional Shock Wave/Turbulent Boundary Layer Interactions," *AIAA Journal*, Vol. 21, No. 3, 1983, pp. 390–397.

[14]Tanner, L. H., and Blows, L. G., "A Study of the Motion of Oil Films on Surfaces in Air Flow, with Application to the Measurement of Skin Friction," *Journal of Physics E: Scientific Instruments*, Vol. 9, No. 3, 1976, pp. 194–202.

[15]Tanner, L. H., "A Skin Friction Meter, Using the Viscosity Balance Principle, Suitable for Use with Flat or Curved Metal Surfaces," *Journal of Physics E: Scientific Instruments*, Vol. 10, No. 3, 1977, pp. 278–284.

[16]Tanner, L. H., "Skin Friction Measurement by Viscosity Balance in Air and Water Flows," *Journal of Physics E: Scientific Instruments*, Vol. 12, No. 7, 1979, pp. 610–619.

[17]Tanner, L. H., and Kulkarni, V. G., "The Viscosity Balance Method of Skin Friction Measurement: Further Developments Including Applications to Three-Dimensional Flow," *Journal of Physics E: Scientific Instruments*, Vol. 9, No. 12, 1976, pp. 1114–1121.

[18]Monson, D. J., and Higuchi, H., "Skin Friction Measurements by a Dual-Laser-Beam Interferometer Technique," *AIAA Journal*, Vol. 19, No. 6, 1981, pp. 739–744.

[19]Monson, D. J., Driver, D. M., and Szodruch, J., "Application of a Laser Interferometer Skin-Friction Meter in Complex Flows," *Proceedings of the International Congress on Instrumentation in Aerospace Simulation Facilities*, Inst. of Electrical and Electronics Engineers Pub. 8/CH1712-9, 1981, pp. 232–243.

[20]Monson, D. J., "A Nonintrusive Laser Interferometer Method for Measurement of Skin Friction," *Experiments in Fluids*, Vol. 1, No. 1, 1983, pp. 15–22.

[21]Westphal, R. V., Bachalo, W. D., and Houser, M. H., "Improved Skin Friction Interferometer," NASA TM 88216, March 1986.

[22]Murphy, J. D., and Westphal, R. V., "The Laser-Interferometer Skin-Friction Meter—A Numerical and Experimental Study," *Proceedings of the Third Symposium on Numerical and Physical Aspects of Aerodynamic Flows* (Long Beach, CA), Jan. 1985, Paper 7-1.

[23]Garrison, T. J., and Settles, G. S., "Improved Methods for Skin Friction Measurements in Compressible Flows by Laser Interferometry," *Experiments in Fluids* (to be submitted for publication).

[24]Van Driest, E. R., "Problem of Aerodynamic Heating," *Aeronautical Engineering Review*, Vol. 15, No. 10, 1956, pp. 26–41.

[25]Wilcox, D. C., "EDDYBL Code User's Guide," DCW Industries, Inc., Rept. DCW-R-NC-04, Oct. 1990.

[26]Sun, C. C., and Childs, M. E., "A Modified Wall Wake Velocity Profile for Compressible Boundary Layers," *Journal of Aircraft*, Vol. 10, No. 6, 1973, pp. 381–383.

[27]Narayanswami, N., Knight, D. D., and Horstman, C. C., "Investigation of a Hypersonic Crossing Shock Wave/Turbulent Boundary Layer Interaction," *Shock Waves*, Vol. 3, No. 1, 1993, pp. 35–48.

[28]Narayanswami, N., Horstman, C. C., and Knight, D. D., "Numerical Simulation of Crossing Shock/Turbulent Boundary Layer Interaction at Mach 8.3—Comparison of Zero- and Two-Equation Turbulence Models," AIAA Paper 93-0779, Jan. 1993.